Electrical injection, continuous wave operation of subwavelength-metallic-cavity lasers at 260K

Electrical injection, continuous wave operation of subwavelength-metallic-cavity lasers at 260 K

Kang Ding,[1] Zhicheng Liu,[1] Leijun Yin,[1] Hua Wang,[1] Ruibin Liu,[1] Martin T. Hill,[2] Milan J. H. Marell,[2] Peter J. van Veldhoven,[2] Richard Nötzel,[2] and C. Z. Ning[1,a)]
[1]*School of Electrical, Computer, and Energy Engineering, Arizona State University, Tempe, Arizona 85287, USA*
[2]*COBRA Research Institute, Technische Universiteit Eindhoven, 5600 MB Eindhoven, The Netherlands*

(Received 22 March 2011; accepted 19 May 2011; published online 8 June 2011)

We report continuous wave lasing operation at T=260 K of subwavelength-metallic-cavities with semiconductor core encapsulated in silver under electric injection. The physical cavity volumes of the two lasers presented are $0.96\lambda^3$ ($\lambda=1563.4$ nm) and $0.78\lambda^3$ ($\lambda=1488.7$ nm), respectively. Longitudinal modes observed in one of lasers correspond to the Fabry–Perot cavity in the length direction. Such record high temperature operation of a subwavelength laser is of great importance for the development of small light sources in future integrated photonic circuits and other on-chip applications. © *2011 American Institute of Physics*. [doi:10.1063/1.3598961]

Microcavity and nanocavity lasers are the research frontier in both the areas of photonics and nanotechnology[1] for its interesting properties in low-dimension physics[2–4] and its appealing prospect in integrated photonics circuits[5,6] and other on-chip applications.[7,8] In the last decade, several types of small laser have been demonstrated such as photonics crystal lasers,[9] microdisk lasers,[10] and photonic wire lasers.[11] However, further scaling down of such dielectric cavity laser becomes exceedingly challenging, and the wavelength becomes the fundamental roadblock.[1] Metallic structures have been designed to manipulate light on subwavelength scale, by exploiting surface plasmons.[12] Despite the common concern of high ohmic losses in metals at optical frequencies when the semiconductor-metal core-shell design was first proposed,[13] it was demonstrated by a detailed study taking into account of the full plasmonic dispersion that the net modal gain can be positive. Any remaining doubt about metallic structure was quickly removed by the first experimental demonstration by Hill *et al.*[14,15] For any practical applications, a subwavelength metallic nanolaser should be able to operate under continuous wave (cw) electrical injection at room temperature. Currently, reported metallic lasers are limited to optical pumping,[16–21] larger dimension than wavelength,[22] or cw lasing at liquid nitrogen temperature or room temperature operation under pulse current injection.[23] Achieving cw lasing under electrical injection at operating temperatures higher than liquid nitrogen temperature would be an important milestone in eventually realizing room temperature lasing.

In this letter we report cw operation of two subwavelength-metallic-cavity lasers at record high temperatures of 260 K under electrical injection. Since such temperatures can be achieved by thermoelectric cooling, realization of cw operation at such temperatures is of great importance for the development of metallic nanolasers, eventually useful for practical applications such as on-chip communications for future computers and for biosensing and chemical sensing and detection.

Our device structure consists of an n-InP/InGaAs/p-InP rectangular pillar with InGaAs as the gain medium as shown in Fig. 1. The semiconductor pillar is then covered by a thin SiN layer from all four sidewalls for insulating purpose. Metallic cavity is formed by encapsulating the pillar core in silver. The detailed device structure as shown in Fig. 1 and fabrication process are described in our previous work.[23]

Devices were mounted on a copper block thermal sink, which formed the p-contact and loaded into a cryostat with liquid nitrogen cooling. The temperature was controlled by an electric heater to 260 K. During measurement, each device was forward biased by a dc voltage source. Emission escaping from the backside of the device substrate was collected by an objective and detected by a spectrometer equipped with a liquid nitrogen cooled InGaAs array detector. The light output versus current (L-I curve) for a device with a volume of 1.1 μm(width) $\times$ 2.15 μm(length) $\times$ 1.55 μm(height) = 0.96 λ^3 ($\lambda=1563.4$ nm) is shown in Fig. 2(a). Figure 2(b) shows the spectra at different currents from this device. The threshold current is estimated at 620 μA. Around threshold, the full width at the half maximum (FWHM) of the lasing peak is 3.78 nm, corresponding to a cavity quality (Q) factor of 416. The FWHM continuously decreases to 1.4 nm at 1712 μA and increases afterwards due to severe self-heating effect at high injection cur-

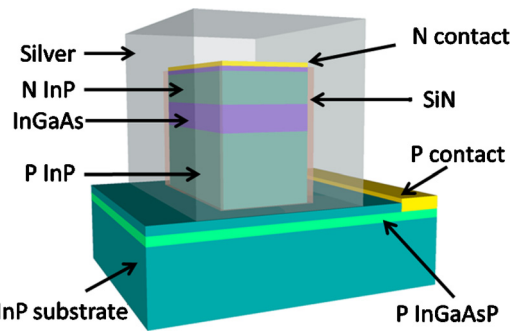

FIG. 1. (Color online) Schematic of the metal-semiconductor nanolaser. InP/InGaAs heterostructure pillar of a rectangular cross section is coated with SiN from the sides before is encapsulated in silver to form a metallic cavity, see text for more explanation.

a)Author to whom correspondence should be addressed. Electronic mail: cning@asu.edu.

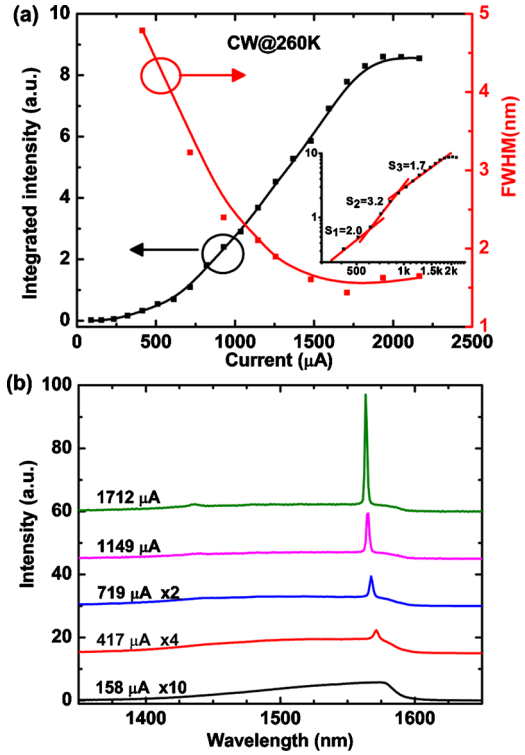

FIG. 2. (Color online) (a) L-I curve from a device with a total volume of $0.96\lambda^3$ at 260 K under dc current injection. The lasing mode shows a threshold around 620 μA. Inset is the L-I curve in log–log scale. (b) Spectra (vertically offset for clarity) at different currents of the same device.

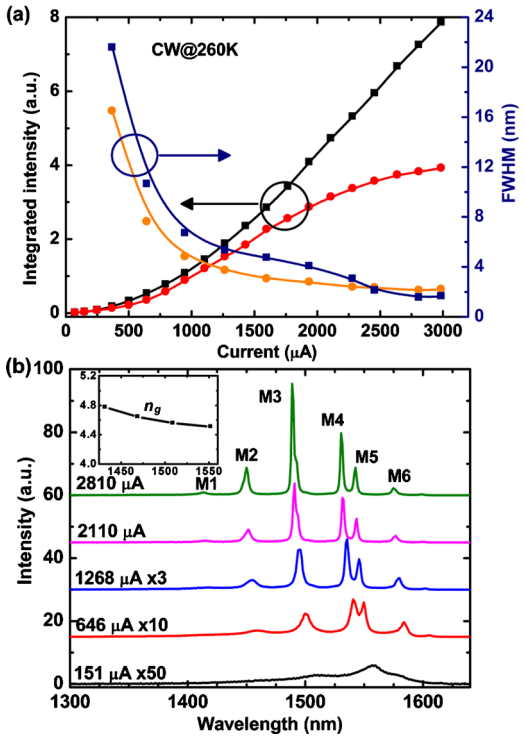

FIG. 3. (Color online) (a) L-I curve and FWHM of the dominant modes M3 (rectangular symbols) and M4 (filled circles) from the second device with volume of $0.78\lambda_3$ at 260 K under dc current injection. Threshold of M3 is around 750 μA while its linewidth drops to 1.55 nm at 2810 μA. (b) Spectra (vertically offset for clarity) at different currents of second device. Multiple modes emerge at high current. Inset is group index calculated using Eq. (1) for longitudinal modes M1–M4 and M6. Here λ is defined as $(\lambda_1\lambda_2)^{1/2}$. The slowly changing n_g verifies the calculation.

rent, which can be reflected from the saturation of integrated lasing mode intensity. Thus both the linewidth and L-I curve show consistently the laser threshold transitions. The lasing peak also exhibits a strong blueshift, from 1573.5 nm at 324 μA to 1563.4 nm at 1712 μA, which can be attributed band filling and possible decrease in refractive index in InP and InGaAs under high carrier injection.[24] The L-I curve is shown in the inset of Fig. 2(a) in log–log scale. Below threshold, the L-I curve shows a slope of 2. This is the typical behavior of spontaneous emission when carrier density linearly increases with injection current. Such linear scaling of current with carrier density suggests that nonradiative recombinations such as surface recombination and Shockley–Read–Hall recombination are the dominant recombination mechanisms in the device below threshold. In the threshold transition region, the L-I shows a larger slope of 3.2. The slope decreases to 1.7 after threshold. The overall changes in slopes with pumping are consistent with the typical threshold behavior of a laser. The only difference is that the slope after the threshold does not reach an asymptotic value of 1, which occurs when the laser is far above threshold. This is due to heating effects that prevent lasing from operation far away above threshold.

Multimode lasing was observed on devices with narrow width but extended length under cw electrical injection. Figure 3(b) shows the spectra at different currents from a device with a volume of 280 nm(width)$\times$6 μm(length) $\times$1.53 μm(height)=0.78 λ^3 (λ=1488.7 nm) at 260 K. Multiple modes [marked as M1–M6 in Fig. 3(b)] emerge at high injection current. Mode M4 initially shows narrower linewidth but saturates afterwards giving way to the final dominant mode M3. From the L-I curve [Fig. 3(a)], the threshold for the M3 is estimated at 750 μA. The continuous decreasing of linewidth to 1.55 nm at 2810 μA confirms the lasing behavior. The linewidth around threshold is 8.22 nm, corresponding to a much smaller Q-factor of 181 compared to the first device. This smaller cavity quality factor can be attributed to not only the smaller volume but also the much narrower width of this device, which leads to a larger surface to volume ratio. It is interesting to relate the difference in cavity Q-factors to the loss mechanisms of two devices. In addition to the typical background loss of the semiconductors involved, there are several surface-related loss processes. The first is the surface roughness scattering loss of photons, which leads to direct decrease in Q-factor; The second process is the metal loss. Due to very shallow skin depth, this is essentially a surface process. The third is the surface recombination of carriers. This process increases the threshold current, resulting in more heat generation, which leads to elevated level of metal loss. Including only the side silver-SiN interfaces, the surface to volume ratios for devices 1 and 2 are 2.67 μm^{-1} and 6.58 μm^{-1}, respectively. Since all the above loss mechanisms are surface-related in nature, the loss is expected to strongly depend on the surface to volume ratio. The loss ratio of the two devices is 0.41 (2.67/6.58). This correlates well with the ratio of the quality factors of the two devices being 1/0.44 (416/181), indicating those surface-related loss mechanisms are likely the major loss difference between the two devices. Other factors may play some roles too, such as unequal surface conditions and surface qualities for two devices that were produced during different fabrication runs. Excluding M5, other modes show a

gradually increasing mode spacing from 36.8 to 44.5 nm, indicating they are Fabry–Perot modes, corresponding to the length direction of the laser cavity. Inset of Fig. 3(b) shows the group index calculated using the standard formula

$$n_g = \frac{\lambda_1 \lambda_2}{2L(\lambda_1 - \lambda_2)}, \quad (1)$$

where $L=6\ \mu m$ is the length of the laser cavity. The group index varies from 4.77 to 4.50. Such high group index is consistent with our two-dimensional simulation for the TE-like mode in the laser metal-insulator-semiconductor-insulator-metal (MISIM) waveguide using a material dispersion $\partial\varepsilon_r/\partial\omega \sim 4\times10^{-15}$ s (Ref. 25) of InGaAs. Through polarization measurement at 100 K, we found that the M5 has a different polarization than other modes and the E field is polarized perpendicular to the propagation direction (the length direction) of the cavity. This suggests that M5 is the TM-like mode, or so called plasmonic gap mode in this MISIM waveguide.[26]

In summary, we demonstrated cw operation of two metallic cavity lasers under electric injection at record high temperature of 260 K. Both devices have physical volumes smaller than the cubic of the operating wavelengths in vacuum. Especially, the second device has a width of cavity smaller than the lasing mode wavelength even inside the gain media. Our results prove that such metallic-cavity structure is capable of minimizing laser device down to subwavelength scale while keeping the cavity loss at a moderate level. It is important to note that the lasers can operate at temperatures that are reachable by thermoelectric cooling range. We believe that these metallic cavity lasers will be important as the on-chip light source in the integrated photonic circuits and for other on-chip optical applications. This operating temperature also represents a milestone in the process of eventually reaching room temperature operation. Currently, the device operation temperature is limited by the insufficient heat dissipation. Improvement of device structure design, fabrication processes, and thermal packaging will be the key to realize cw operation at room temperature.

This work was supported by the Defense Advanced Research Project Agency (DARPA) program Nanoscale Architectures of Coherent Hyper-Optical Sources (NACHOS, Grant No. W911-NF07-1-0314) and by the Air Force Office of Scientific Research (Grant No. FA9550-10-1-0444, Gernot Pomrenke).

[1] C. Z. Ning, Phys. Status Solidi B **247**, 774 (2010).
[2] Y. Yamamoto and S. Machida, Phys. Rev. A **44**, 657 (1991).
[3] J. M. Gérard, B. Sermage, B. Gayral, B. Legrand, E. Costard, and V. Thierry- Mieg, Phys. Rev. Lett. **81**, 1110 (1998).
[4] J. Vučković and Y. Yamamoto, Appl. Phys. Lett. **82**, 2374 (2003).
[5] D. A. B. Miller, Proc. IEEE **97**, 1166 (2009).
[6] P. Rojo Romeo, J. van Campenhout, P. Regreny, A. Kazmierczak, C. Seassal, X. Letartre, G. Hollinger, D. van Thourhout, R. Baets, J. M. Fedeli, and L. Di Cioccio, Opt. Express **14**, 3864 (2006).
[7] M. Lončar, A. Scherer, and Y. Qiu, Appl. Phys. Lett. **82**, 4648 (2003).
[8] W. Fang, D. B. Buchholz, R. C. Bailey, J. T. Hupp, R. P. H. Chang, and H. Cao, Appl. Phys. Lett. **85**, 3666 (2004).
[9] H. Park, S. Kim, S. Kwon, Y. Ju, J. Yang, J. Baek, S. Kim, and Y. Lee, Science **305**, 1444 (2004).
[10] K. Srinivasan, M. Borselli, O. Painter, A. Stintz, and S. Krishna, Opt. Express **14**, 1094 (2006).
[11] J. P. Zhang, D. Y. Chu, S. L. Wu, S. T. Ho, W. G. Bi, C. W. Tu, and R. C. Tiberio, Phys. Rev. Lett. **75**, 2678 (1995).
[12] S. I. Bozhevolnyi, V. S. Volkov, E. Devaux, J.-Y. Laluet, and T. W. Ebbesen, Nature (London) **440**, 508 (2006).
[13] A. V. Maslov and C. Z. Ning, Proc. SPIE **6468**, 64680I (2007).
[14] M. T. Hill, Y. S. Oei, B. Smalbrugge, Y. Zhu, T. de Vries, P. J. van Veldhoven, F. W. M. van Otten, T. J. Eijkemans, J. P. Turkiewicz, H. de Waardt, E. J. Geluk, S. Kwon, Y. Lee, R. Nötzel, and M. K. Smit, Nat. Photonics **1**, 589 (2007).
[15] M. T. Hill, J. Opt. Soc. Am. B **27**, B36 (2010).
[16] R. F. Oulton, V. J. Sorger, T. Zentgraf, R. M. Ma, C. Gladden, L. Dai, G. Bartal, and X. Zhang, Nature (London) **461**, 629 (2009).
[17] M. P. Nezhad, A. Simic, O. Bondarenko, B. Slutsky, A. Mizrahi, L. Feng, V. Lomakin, and Y. Fainman, Nat. Photonics **4**, 395 (2010).
[18] K. Yu, A. Lakhani, and M. Wu, Opt. Express **18**, 8790 (2010).
[19] S. Kwon, J. Kang, C. Seassal, S. Kim, P. Regreny, Y. Lee, C. M. Lieber, and H. Park, Nano Lett. **10**, 3679 (2010).
[20] M. A. Noginov, G. Zhu, A. M. Belgrave, R. Bakker, V. M. Shalaev, E. E. Narimanov, S. Stout, E. Herz, T. Suteewong, and U. Wiesner, Nature (London) **460**, 1110 (2009).
[21] R. Perahia, T. P. Mayer, A. H. Safavi-Naeini, and O. Painter, Appl. Phys. Lett. **95**, 201114 (2009).
[22] C. Y. Lu, S. W. Chang, S. L. Chuang, T. D. Germann, and D. Bimberg, Appl. Phys. Lett. **96**, 251101 (2010).
[23] M. T. Hill, M. Marell, E. S. P. Leong, B. Smalbrugge, Y. Zhu, M. Sun, P. J. van Veldhoven, E. J. Geluk, F. Karouta, Y. S. Oei, R. Nötzel, C. Z. Ning, and M. K. Smit, Opt. Express **17**, 11107 (2009).
[24] B. R. Bennett, R. A. Soref, and J. A. D. Alamo, IEEE J. Quantum Electron. **26**, 113 (1990).
[25] S. Adachi, J. Appl. Phys. **66**, 6030 (1989).
[26] N. Feng, M. L. Brongersma, and L. D. Negero, IEEE J. Quantum Electron. **43**, 479 (2007).